




Imaging of vitreous cortex hyalocyte dynamics using non-confocal quadrant-detection adaptive optics scanning light ophthalmoscopy in human subjects: supplement

JUSTIN V. MIGACZ,¹ OSCAR OTERO-MARQUEZ,¹ REBECCA ZHOU,¹ KARA RICKFORD,¹ BRIAN MURILLO,¹ DAVIS B. ZHOU,¹ MARIA V. CASTANOS,¹ NRIPUN SREDAR,²  ALFREDO DUBRA,²  RICHARD B. ROSEN,¹ AND TOCO Y. P. CHUI^{1,*} 

¹Department of Ophthalmology, The New York Eye and Ear Infirmary of Mount Sinai, New York, NY 10003, USA

²Department of Ophthalmology, Stanford University, Palo Alto, CA 94303, USA

*ychui@nyee.edu

This supplement published with Optica Publishing Group on 1 March 2022 by The Authors under the terms of the [Creative Commons Attribution 4.0 License](https://creativecommons.org/licenses/by/4.0/) in the format provided by the authors and unedited. Further distribution of this work must maintain attribution to the author(s) and the published article's title, journal citation, and DOI.

Supplement DOI: <https://doi.org/10.6084/m9.figshare.19207170>

Parent Article DOI: <https://doi.org/10.1364/BOE.449417>

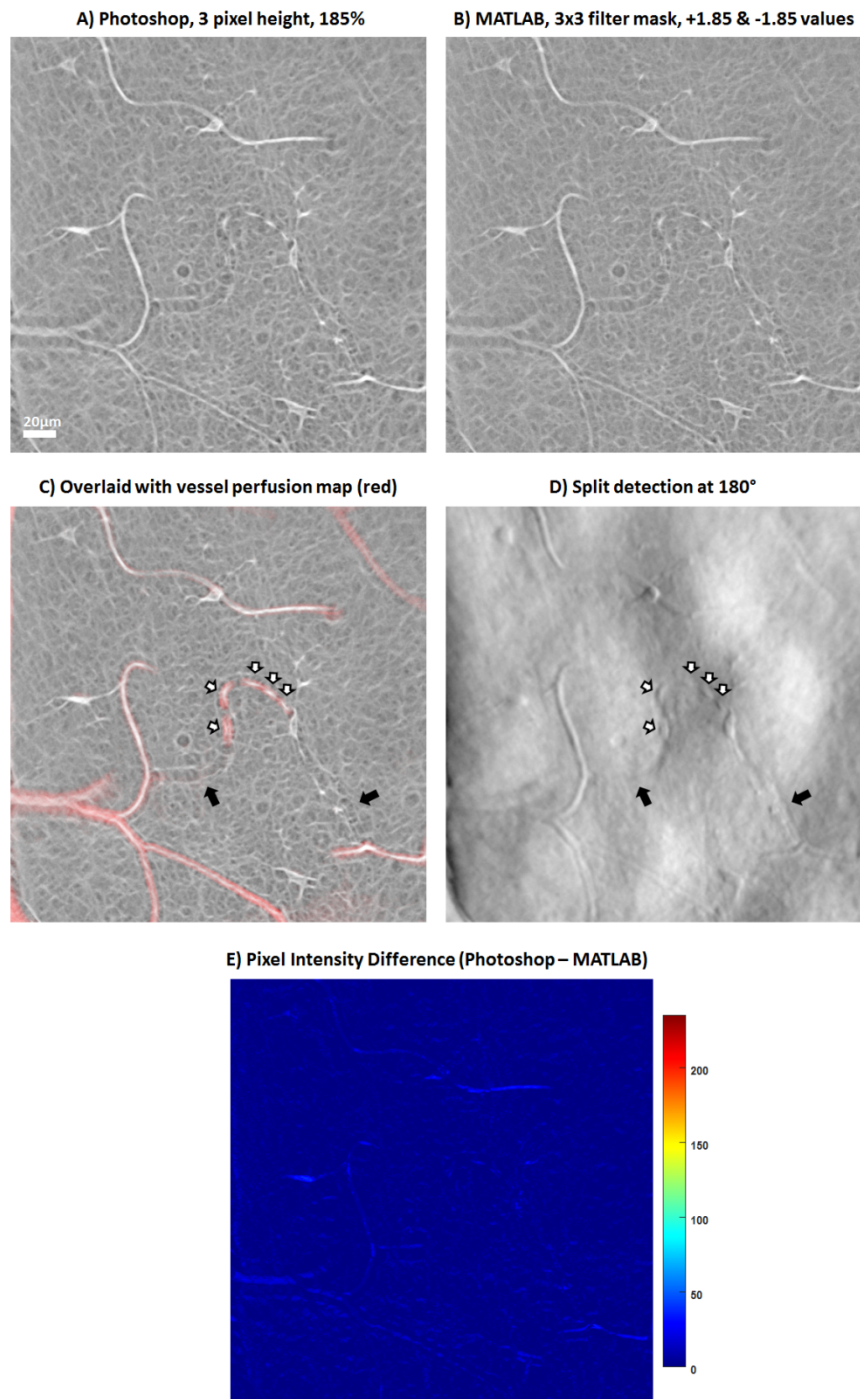


Fig. S1. Comparison of merged emboss-filtered image processed using A) Photoshop and B) MATLAB with similar parameters. C) Merged emboss-filtered image overlaid with the averaged vessel perfusion map (red) generated using motion contrast computation of the 4 split-detection videos. D) Split-detection image at 180°. Black arrows indicate two nonperfused capillary segments; white arrows indicate red blood cells which were momentarily stuck inside a capillary during the acquisition. E) Pixel intensity difference of the images in A & B.

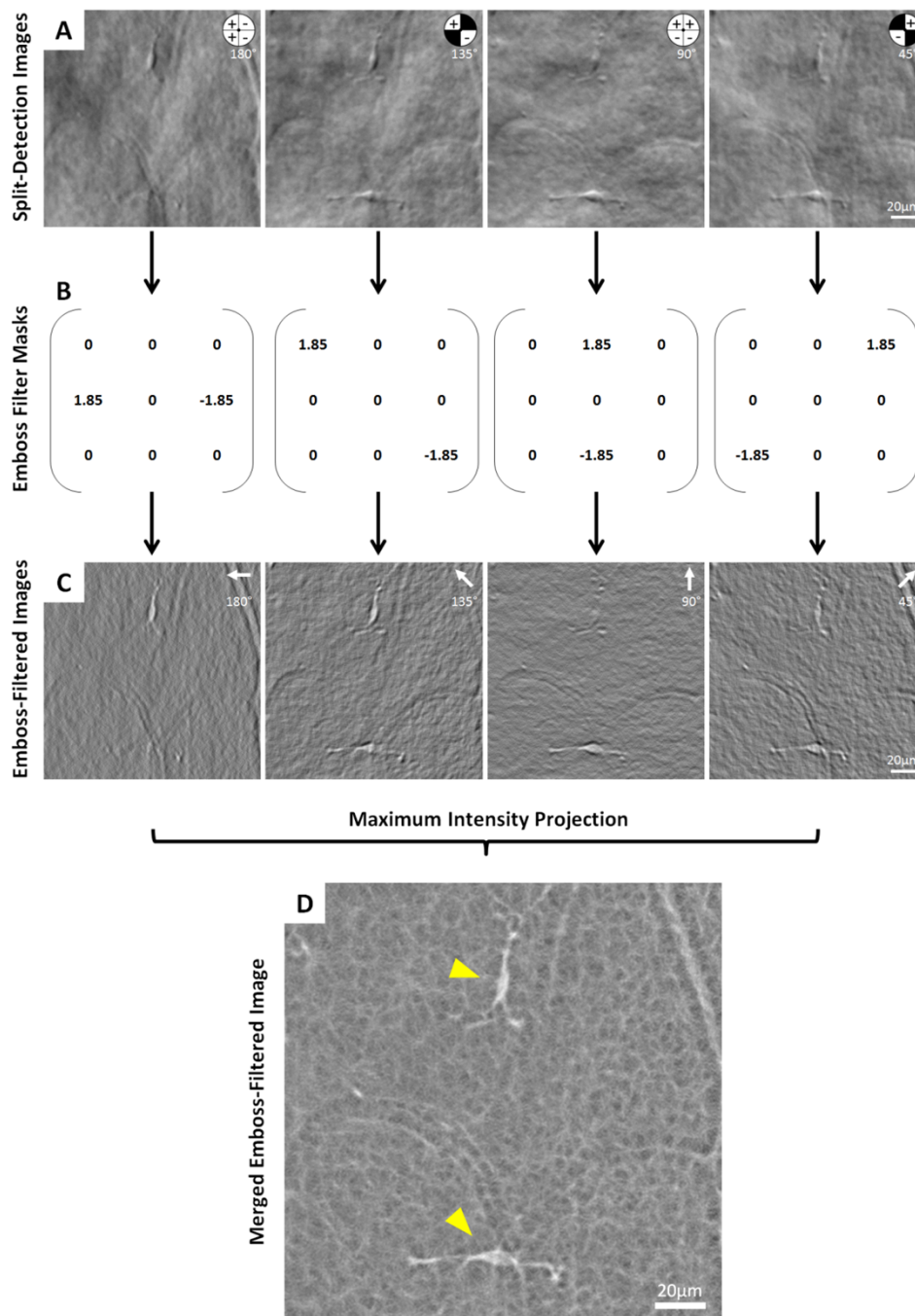


Fig. S2. Emboss filtering of split-detection images using MATLAB. A) Split-detection images at 180°, 135°, 90°, & 45°. B) 3x3 emboss filter masks with +1.85 and -1.85 in 4 directions. The emboss filter mask was in convolution calculation with the corresponding split detection image, resulting in C) 4 emboss-filtered images with edge enhancement orthogonal to the mask direction. D) The 4 emboss-filtered images were then merged into a single image using maximum intensity projection, which provides high contrast visualization of both hyalocytes and their processes in the same image (arrowheads) and reveals the complex meshwork structure of the surrounding.

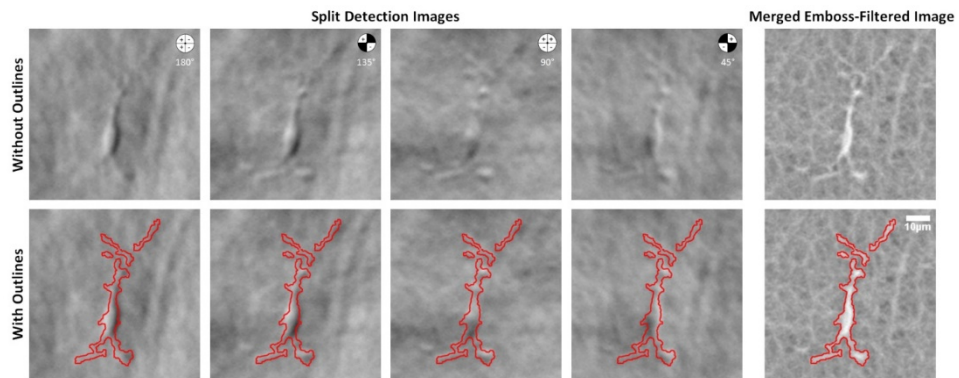


Fig. S3. Comparison between the 4 split-detection and the merged emboss-filtered images of the same hyalocyte. Top row: cell without segmentation outlines. Bottom row: cell segmentation (in red) was performed manually on the merged emboss-filtered image using Photoshop (magic wand tool with 50% tolerance). Cell outlines were then overlaid on the 4 split detection images.

Histograms of Cumulative Path Length Measured Over 2 Hours with 30 Min Intervals

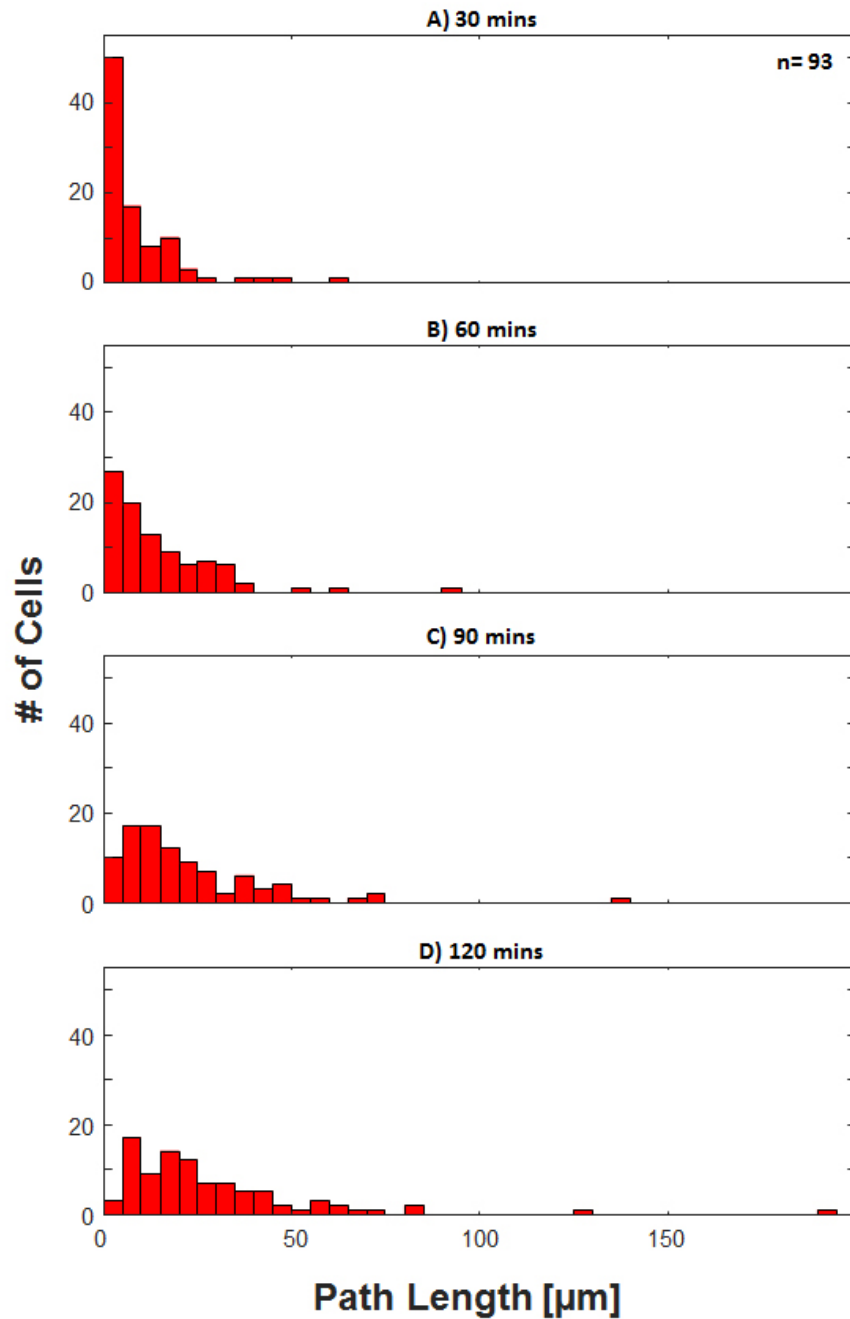


Fig. S4. Histograms of cumulative path length measured at 4 time points over 2 hours at 30-minute intervals. Total number of hyalocytes = 93.

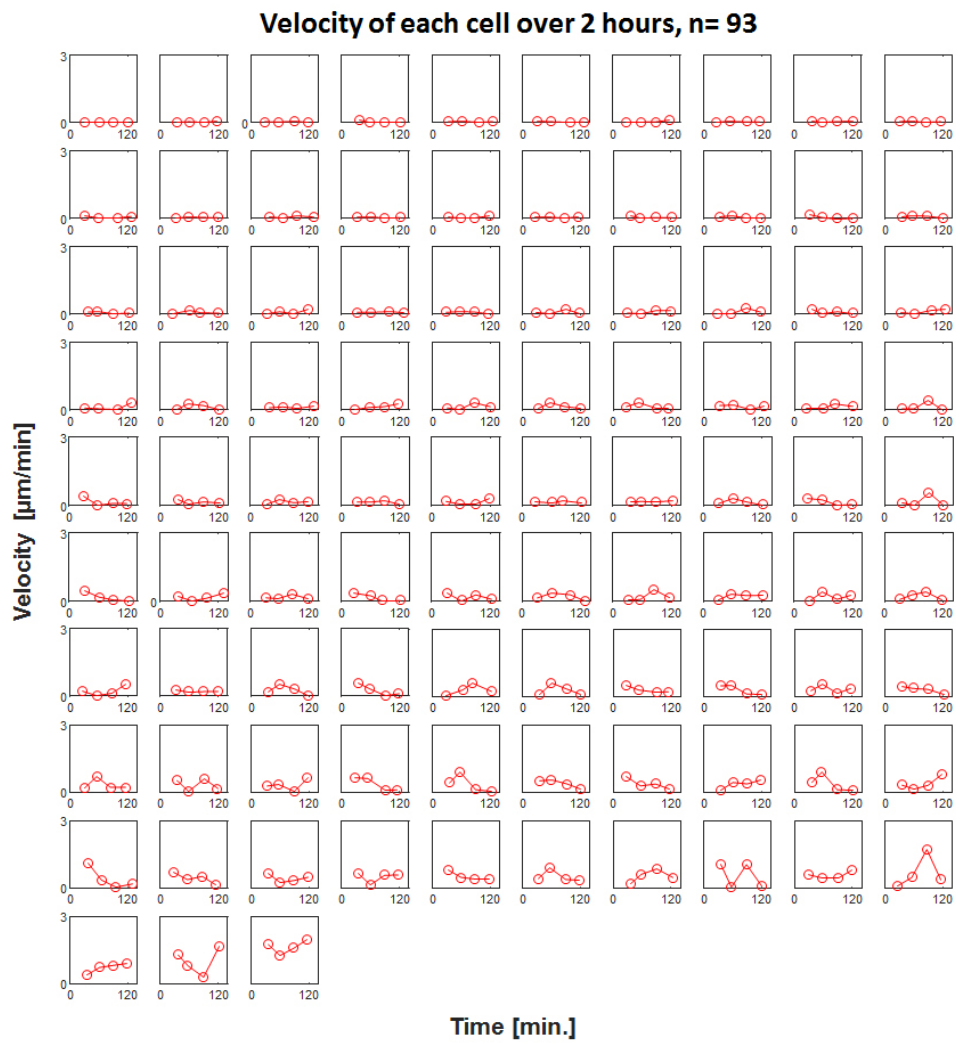


Fig. S5. Individual velocity plots for 93 hyalocytes tracked over 2 hours at 30-minute intervals. The traces were presented individually to prevent the crowding shown in the main manuscript.

Histograms of Cumulative Path Length Measured Over 1 Hour with 5 Min Intervals

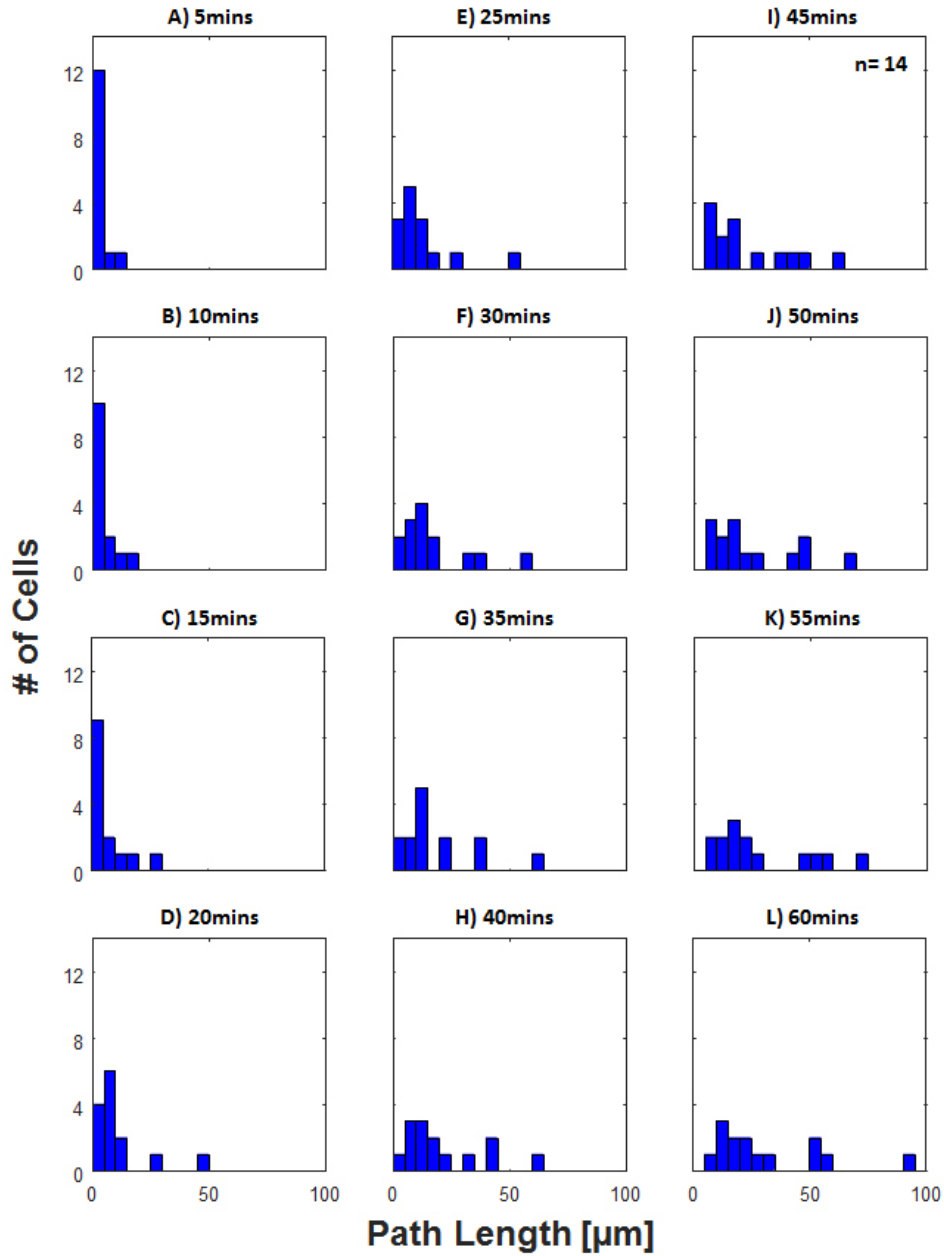


Fig. S6. Histograms of cumulative path length measured at 12 time points over 1 hour at 5-minute intervals. Total number of hyalocytes = 14.

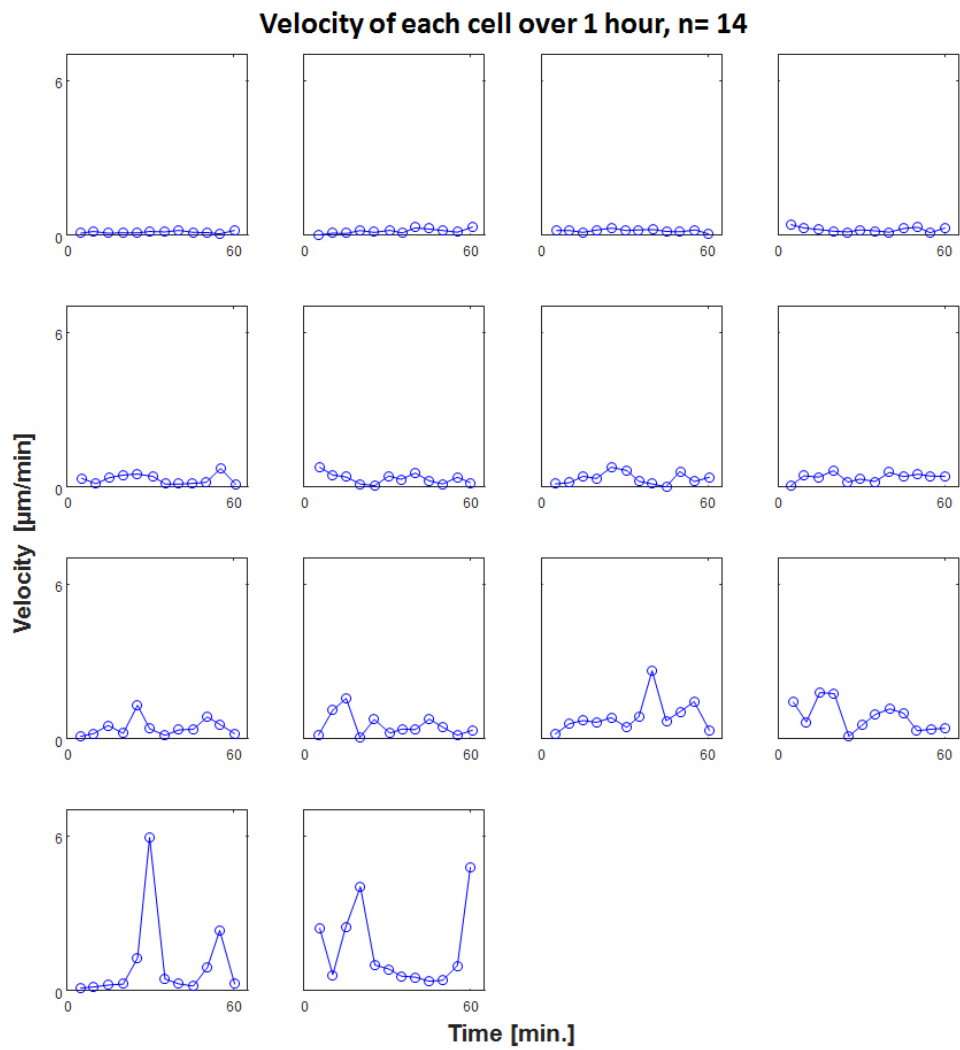


Fig. S7. Individual velocity plots for 14 hyalocytes tracked over 1 hour at 5-minute intervals. The traces were presented individually to prevent the crowding shown in the main manuscript. Also, most cells show little movement, and when larger movement occurs, it is usually brief.